Indirect Excitation of micro-HRG Using Segmented Piezoelectric ALD PHT Actuator

Danmeng Wang[1], Nicholas A. Strnad[2], Yusheng Wang[1], Austin R. Parrish[1], Robert R. Benoit[2], Ryan R. Knight[2], and Andrei M. Shkel[1]
[1]MicroSystems Laboratory, University of California, Irvine, CA, USA
[2]DEVCOM Army Research Laboratory, Adelphi, MD, USA

Abstract*—This paper presents, for the first time, an indirect excitation method for three-dimensional fused quartz dual-shell micro-scale Hemispherical Resonator Gyroscope (μHRG). The μHRG was fabricated using three wafer bonding and high-temperature micro-glassblowing processes, providing a sensing element (device shell), a self-aligned fixed-fixed anchor for increased immunity to mechanical shocks and vibrations, and a housing (cap shell) for vacuum encapsulation. The novel actuation technique uses piezoelectric actuation to transfer energy from the cap shell to the device shell to excite the resonant element, where the piezoelectric material is deposited and shaped on the outer cap shell. Using the proposed indirect excitation method, the metal coating of the device shell is eliminated, preserving the high quality factor of the pristine fused quartz material. In this paper, we first introduce the mechanism of excitation, supported by Finite Element Analysis (FEA). We then describe the Atomic Layer Deposition (ALD) method of $PbHf_xTi_{1-x}O_3$ (PHT) piezoelectric material, followed by the fabrication process of a dual-shell μHRG prototype co-fabricated with an 80 nm layer of ALD PHT actuator. Finally, we experimentally demonstrated the indirect excitation, showing the feasibility of the method as a possible alternative to capacitive or direct piezoelectric actuation. Though early in development, the reported excitation approach may offer a preferable method for excitation of μHRGs, allowing to achieve the ultra-high mechanical quality factor, on the level of the TED-limit of fused quartz.

Keywords: Fused Quartz, Hemispherical Resonator Gyroscope, Dual-Shell Gyroscope, Metallization, Quality factor, Piezoelectric, ALD PHT

I. Introduction

The quality factor (Q-factor) is a key parameter of MEMS Coriolis Vibratory Gyroscopes (CVGs) that is directly related to the gyroscope's sensitivity, power consumption, and noise characteristics [1], [2]. Many factors influence the overall Q-factor of the resonators, such as viscous air damping, thermoelastic dissipation (TED), anchor losses, and surface-related losses. Among them, TED represents the upper-limit and was reported to dominate the Q-factor in the kHz range of micro-scale resonators, showing an inverse relationship between the Q-factor and the material's internal friction [3]. A fabrication approach for CVGs utilizing Fused Quartz (FQ) as the structural material has emerged in recent years. Recently, FQ μHRGs fabricated using the glassblowing technology, and its variations, demonstrated as-fabricated Q-factors on the order of a few millions [4], [5].

This material is based on work supported by the U.S. Army Research Laboratory under Grant W911NF2220069.

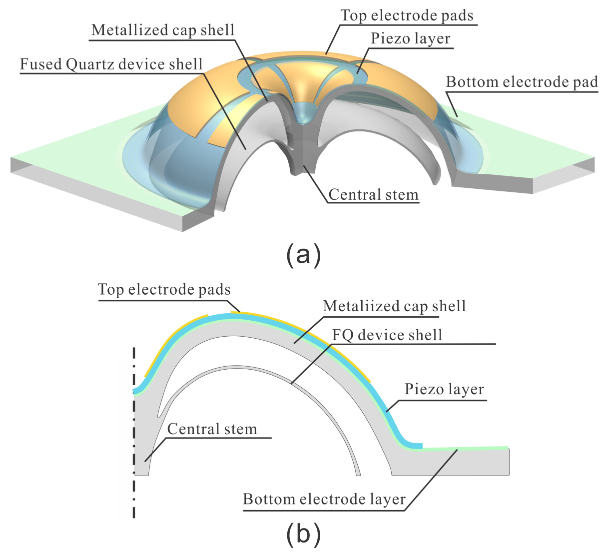

Fig. 1. Schematics of (a) a Fused Quartz Dual-Shell Gyroscope and (b) a cross-section view, illustrating the sensing element (metal-free device shell), the central anchor, and the metallized outer cap shell with a three-layer piezoelectric stack for indirect excitation. The central anchor and cap shell form a self-aligned fixed-fixed double-ended anchor for the device shell.

To implement the μHRGs from FQ to operate as a CVG, two common methods have been explored for vibrational excitation of μHRGs: (1) capacitive electrostatic actuation [6] and (2) direct piezoelectric actuation [7]. Both methods require one or multiple layers of metal thin-films coating of the sensing element of μHRGs to bias the proof-mass and form the piezoelectric actuation stack, correspondingly. The metallization would typically reduce the structural Q-factor by about five times due to significantly increased surface losses and additional metal film stresses [6], [8]. Therefore, an alternative actuation implementation was thought to eliminate the metal coating process and achieve the theoretical TED-limit of the pristine FQ material.

We report, for the first time, an indirect excitation method of the FQ Dual-Shell μHRGs (DSGs), which does not require metallization of the sensing element (device shell). The proposed actuation method is readily compatible with photonic detection, this is the subject of active current research, and therefore will be not discussed in this paper. The DSG consists of two hemispherical shells simultaneously co-fabricated using a triple-stack micro-glassblowing process of the FQ material.

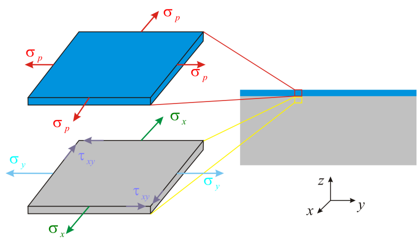

Fig. 2. Stress of differential volume elements on the surface of the piezoelectric resonator, where the dual-layer is formed by the excited piezoelectric material (blue) and the resonator material (gray).

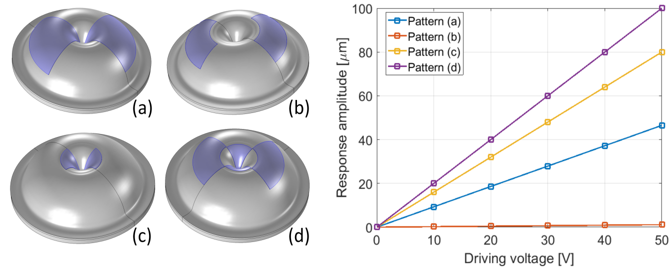

Fig. 3. The comparison of different electrode shape configurations. The predicted maximum displacements of the dual-shell resonator under each case are shown on the right as a function of driving voltages.

The process was disclosed in our patents [9], [10] and experimentally demonstrated in our recent publications [5], [6]. As shown in Fig. 1, the inner device shell is sensitive to inertial rotations, and the outer cap shell provides housing for sensor packaging. The cap shell and the central stem form a double-ended anchor to improve the reliability of the sensing element. In this paper, instead of metal-coating on the device shell for capacitive actuation, the indirect excitation method utilizes piezoelectric material deposited on the cap shell and vibration of the cap shell to transfer the energy to the device shell, thus driving the sensing element to resonance.

II. Simulation Analysis

The piezoelectric actuator stack for the proposed indirect excitation of the device shell is deposited on the cap shell formed by a continuous bottom electrode layer, a central piezoelectric layer, and segmented top electrode pads, Fig. 1. The drive voltage is applied between the two electrode layers, and the energy induced by piezoelectric effect is then transferred to the inner device shell through the mechanical coupling between the cap shell and device shell. In order to optimize the geometry of the top piezo electrodes for maximum transduction of vibration of the desired resonant modes, electrode-shaping is the primary design consideration. As shown in Fig. 2, assuming a thin piezoelectric layer on the surface of the resonator, the differential volume elements (σ_1, σ_2, and τ_{xy}) on the surface can be considered to be in the state of plane stress in the x-y plane. For most commonly used piezoelectric materials, such as PZT, AlN, and ZnO, their piezoelectric coefficients e_{31} and e_{32} are the same. Thus, the piezoelectric differential element is in a state of bi-axial stress, with equal and invariant stress components σ_p along any direction. Coordinate transformation can be applied to extract the principal stress of the resonator differential element:

$$\sigma_{1,2} = \frac{\sigma_1 + \sigma_2}{2} \pm \sqrt{(\frac{\sigma_x - \sigma_y}{2})^2 + \tau_{xy}^2} \qquad (1)$$

where σ_1 and σ_2 are two principal stresses along the first and second principal axes. The shear stress τ_{xy} in the modal element is eliminated by the rotation into the principal plane, as described in [11]. The resonant mode in our implementation will be locally excited when the piezoelectrically induced stresses are in-phase with the modal stresses, i.e., when the signs of σ_1, σ_2, and σ_p are the same. Therefore, we can define a parameter β to describe the proposed electrode design:

$$\beta = \begin{cases} sign(\sigma_1)sign(\sigma_p), & \text{if} sign(\sigma_1) = sign(\sigma_p), \\ 0, & \text{if} sign(\sigma_1) \neq sign(\sigma_p). \end{cases} \qquad (2)$$

In the area where β = 0, the local force cancellation will occur since σ_1 and σ_2 are of different signs. However, for the areas corresponding to β = 1 and β = -1, the piezoelectrically induced stress will excite or inhibit the resonance, respectively. Therefore, one set of electrodes can be deposited in the area, where β = 1, to excite the resonance. In contrast, another set of electrodes can be deposited in the area where β = -1, to form the differential driving architecture for a certain resonant mode.

A. Frequency Response of Piezoelectric Resonators

The transduction efficiency of indirect piezoelectric actuation was modeled using Rapid Analytical-FEA Technique (RAFT) [12], where piezoelectric resonators can be considered as an equivalent circuit model. Resonant modes were assumed to be independent of each other, and a full frequency response was obtained by superimposing the response of each mode.

In a quasi-static simulation, there are three types of internal energy stored in a piezoelectric resonator: purely elastic energy U_e, purely electric energy U_d, and the energy due to the piezoelectric effect U_p. In this study, only U_p is considered, which includes the elastic energy generated when an electric field is applied to the piezoelectric material, as well as the capacitive energy due to the deformed piezoelectric material. Since U_p consists of two parts, it was modeled as a lumped spring with a modal force and a lumped capacitor with an applied voltage, and these two parts have the same magnitude. Then, the total energy can be expressed as, [12],

$$\tfrac{1}{2}F_m\delta + \tfrac{1}{2}q\Phi = \Phi\delta \int_V \nabla\phi^T e^t S_n dV, \qquad (3)$$

where F_m is the modal force, δ is the modal displacement, q is the charge in the modal capacitor, Φ is the applied voltage, e is the matrix of piezoelectric stress constants, ϕ is the normalized electric potential field, S_n is the normalized strain field, and V is the volume of the piezoelectric material. Then, the modal force and the effective stiffness can be calculated as

$$F_m = \Phi \int_V e^t \nabla\phi S_n dV, \qquad (4)$$

$$k_m = \int_V S_n^T c^E S_n dV, \tag{5}$$

where c^E is the stiffness matrix. The vibration of the piezoelectric resonator, u, can be expressed as

$$u = \delta \cdot u_n \cdot \frac{e^{j\omega t}}{(1 - \frac{\omega^2}{\omega_n^2}) + \frac{j\omega}{Q_m \omega_n}}, \tag{6}$$

where $\delta = \frac{F_m}{k_m}$ is the static modal displacement, u_n is the normalized mode shape, ω_n is the resonant frequency of the mode, Q_m is the quality factor of the mode, and ω is the driving frequency.

B. Piezoelectric Actuation Simulation

The FQ dual-shell resonator is designed to operate at n = 2 wineglass mode. According to the models, Eq. (2) and Eq. (6), and the mode shape of the n = 2 mode, four different driving configurations were compared in terms of their transduction rate. The results are presented in Fig. 3, where the x-axis is the amplitude of the applied AC voltage, and the y-axis is the corresponding predicted maximum displacement of the resonator. The maximum driving voltage would be limited by PHT thickness in the real case, which was not considered in the simulation. The thickness of the $PbHf_xTi_{1-x}O_3$ (PHT) piezoelectric material on the cap shell was set to be 1 μm. The resonant frequency of the n = 2 mode was assumed to be 15 kHz with a typical Q-factor value of 1×10^5. The optimized electrode pattern (d) showed the highest transduction rate for the n = 2 mode with an amplitude of about 20µm at 10V driving voltage, verifying that it was the optimal design in terms of transduction rate.

III. Fabrication

The DSG with a piezoelectric layer for indirect excitation was realized using a modified triple-wafer high-temperature glassblowing process with an ALD of PHT material. The wafer-level process flow is described in Fig. 4. The dual-shell structure was first formed using the micro-glassblowing process described in steps (a) to (e) in Fig. 4, followed by a surface cleaning using standard Piranha solution to remove any organic residue before the subsequent deposition process. The process has been developed in the MicroSystems Lab at the University of California, Irvine, and the details are discussed in our previous works [5], [6], [9], [10].

The deposition process of the metal-piezoelectric-metal stack actuator on the cap shell was developed and completed in the Specialty Electronic Materials and Sensors Cleanroom (SEMASC) at the DEVCOM Army Research Laboratory (DEVCOM ARL, Adelphi, MD, USA) [13]. The process started with the deposition of a bottom electrode adhesion layer (20 nm Ti) and bottom electrode (100 nm Pt) sequentially using a commercial sputtering platform with 4-inch confocal cathodes and a rotating substrate chuck at room temperature, Step (f). Then, a piezoelectric PHT layer was coated using the ALD technique in a commercial ALD 150-LX platform with a chuck temperature of 275°C. The details of the developed PHT supercycles are presented in Fig. 5. The supercycle was repeated 80 times, yielding an approximately 80 nm

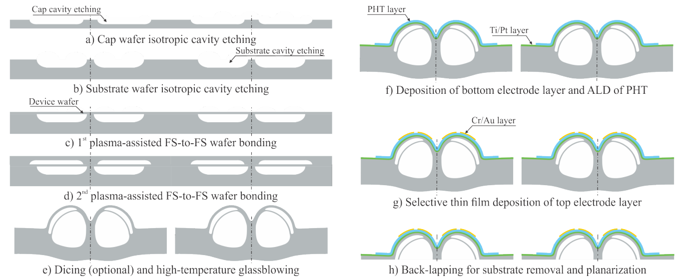

Fig. 4. Process flow for FQ dual-shell architecture with ALD of a piezoelectric PHT stack. The high-temperature glassblowing technology was performed at 1550°C. The substrate is removed and planarized by lapping and CMP for subsequent characterization.

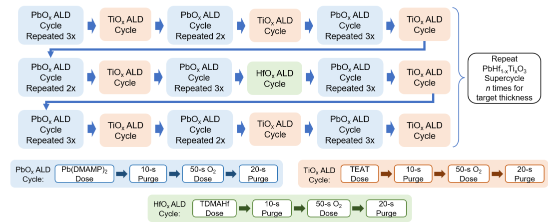

Fig. 5. Schematic diagram of ALD super-cycle for $PbHf_xTi_{1-x}O_3$ layer deposition with a PbO_x:HfO_x:TiO_x cycle ratio of 24:1:8.

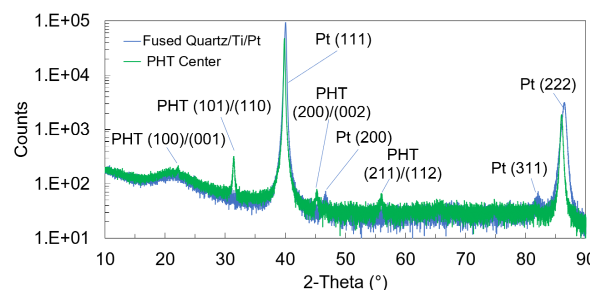

Fig. 6. The experimental results of goniometer 2-theta X-ray diffraction (XRD) scan of two FQ proxy samples. The blue line shows the FQ sample coated with only sputtered Ti and Pt, while the green line shows the FQ sample coated with Ti, Pt, and ALD PHT following the tube furnace crystallization.

PHT layer. The as-grown ALD PHT film was subsequently crystallized into the desired perovskite phase at 525°C for 30-min in pure O_2, followed by a final crystallization anneal. In Step (g), a 100/500 nm Cr/Au layer was selectively deposited using a shadow mask to form the top electrodes on top of the PHT film. Finally, the inner device shell of the DSG was released as the sensing element using a parallel back-lapping step utilizing the Allied HighTech MultiPrep™ polisher, Step (h) in Fig. 4.

In order to evaluate the characteristics of the ALD PHT layer, a flat FQ proxy sample was fabricated using the proposed process flow, steps (f) and (g). A comparison of the crystallinity between the proxy sample and a comparative sample coated with only sputtered Ti and Pt was presented in Fig. 6. The results indicate that the primary PHT peak appears at 31.4° and is attributed to (101) and (110) crystal planes. A small but noticeable peak of either (100) or (001) crystal plane occurs at 22.1°. Figure 7 shows ferroelectric hysteresis loops of the 80 nm ALD PHT layer on the proxy sample

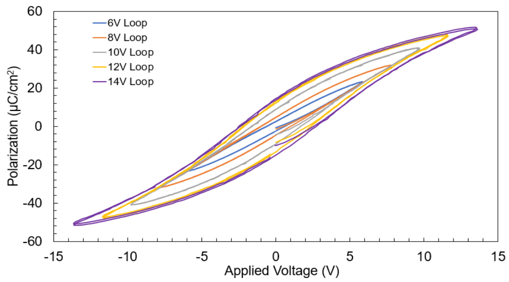

Fig. 7. Nested double-bipolar ferroelectric hysteresis measurements with a test period of 1-ms of each loop, performed on the proxy sample for ALD PHT on FQ with sputtered Ti/Pt electrodes.

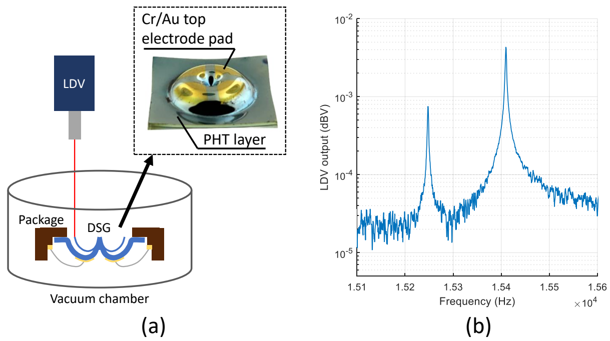

Fig. 8. (a) Experimental setup to acquire (b) frequency response of the FQ dual-shell prototype, measured through indirect piezoelectric actuation and LDV detection.

measured using a Radiant Ferroelectric Tester. As shown in Fig. 7, the ferroelectric switching implies that the films are piezoelectric. The double bipolar loop performed between $\pm$14V shows ferroelectric hysteresis with max polarization of $\pm$ 51.6 μC/cm^2 and remnant polarization of 13.35 and -14.8 μC/cm^2 for positive and negative biases, respectively.

IV. Testing and Characterization

A FQ dual-shell prototype with the co-fabricated 80 nm layer of ALD PHT actuator was formed using the described process flow, shown in Fig. 8(a). In the initial characterization, four segmented Cr/Au top electrode pads were sputter-coated on the cap shell to demonstrate the indirect excitation of the inner device shell. The top electrode pads were first wire-bonded, and the prototype was placed in a vacuum chamber which was pumped down to the pressure level of 0.1 mTorr. The amplitude of motion of the device shell was measured using a Polytech Laser Doppler Vibrometer (LDV), as illustrated in Fig. 8(a). By applying the AC driving voltage across the top and bottom electrodes with the amplitude of 2.5 Vpp, the frequency response, Fig. 8(b), reveals a frequency split on the order 155Hz of the n = 2 wineglass mode actuated using the indirect excitation method.

V. Conclusion

For the first time, a technique has been demonstrated to indirectly excite the resonant element of the micro-dual-shell HRG through the piezoelectric stack deposited on the cap shell. An explanation of the excitation mechanism was supported by a FEA analysis and presented as, potentially, an alternative to the traditional capacitive or direct piezo actuation method, eliminating the undesirable metal-coating effect on the resonator's quality factor. We introduced a detailed fabrication process for realizing such resonators with ALD piezoelectric PHT actuators, followed by an experimental demonstration of the feasibility of the proposed indirect excitation method. The XRD and ferroelectric characterizations of the ALD PHT material were also reported. Current research is pursuing a better understanding of the limitations and advantages of indirect excitation as compared to conventional excitation technologies, as well as tuning and compatible detection methods.

Acknowledgment

Devices were designed and characterized at the UCI Microsystems Laboratory and fabricated at the UCI INRF Cleanroom and the ARL SEMASC Cleanroom. The authors would like to thank James Mulcahy at SEMASC for his help during the fabrication process.

References

[1] D. D. Lynch, "Vibratory gyro analysis by the method of averaging," in *Int. Conf. Gyroscopic Technol. Navigat.*, St. Petersburg, Russia, May 1995.

[2] M. Weinberg, R. Candler, S. Chandorkar, J. Varsanik, T. Kenny, and A. Duwel, "Energy loss in MEMS resonators and the impact on inertial and RF devices," in *IEEE International Solid-State Sens., Actuators Microsyst. (TRANSDUCERS)*, Denver, CO, USA, June 21–25, 2009.

[3] C. Zener, "Internal friction in solids II. General theory of thermoelastic internal friction," *Physical Review*, vol. 53, no. 1, p. 90, 1938.

[4] A. Darvishian, T. Nagourney, J. Y. Cho, and et al., "Thermoelastic dissipation in micromachined birdbath shell resonators," *IEEE/ASME Journal of Microelectromechanical Systems*, vol. 26, no. 4, pp. 758–772, 2017.

[5] M. H. Asadian, D. Wang, and A. M. Shkel, "Fused quartz dual-shell resonator gyroscope," *IEEE/ASME Journal of Microelectromechanical Systems*, vol. 31, no. 4, pp. 533 – 545, 2022.

[6] D. Wang, M. H. Asadian, W. Guan, D. Hii, A. R. Parrish, and A. M. Shkel, "Effect of metallization on quality factor and noise characteristics in fused silica dual-shell gyroscopes," *IEEE/ASME Journal of Microelectromechanical Systems*, vol. 31, no. 6, pp. 877–887, 2022.

[7] P. Chabbi, D. Gautam, and V. K. Rao, "Experimental and numerical studies on mechanical resonance of piezoelectric hemispherical resonator gyroscope," in *IEEE International Conference on Electronics, Computing and Communication Technologies (CONECCT)*, Bangalore, India, July 9-11, 2021.

[8] T. Nagourney, J. Y. Cho, A. Darvishian, and et al., "Effect of metal annealing on the Q-factor of metal-coated fused silica micro shell resonators," in *IEEE International Symposium on Inertial Sensors and Systems (INERTIAL)*, Hapuna Beach, HI, USA, Mar. 23–26, 2015.

[9] A. M. Shkel and D. Senkal, "Environmentally robust micro-wineglass gyroscope," US Patent 9,429,428, Aug. 30, 2016.

[10] A. M. Shkel, M. H. Asadian, and Y. Wang, "Fused quartz dual shell resonator and method of fabrication," US Patent 16,836,387, Oct. 1, 2020.

[11] J. S. Pulskamp, S. S. Bedair, R. G. Polcawich, and et al., "Electrode-shaping for the excitation and detection of permitted arbitrary modes in arbitrary geometries in piezoelectric resonators," *IEEE Transactions on Ultrasonics, Ferroelectrics, and Frequency Control*, vol. 59, no. 5, pp. 1043–1060, 2012.

[12] J. M. Puder, J. S. Pulskamp, R. Q. Rudy, and et al., "Rapid harmonic analysis of piezoelectric mems resonators," *IEEE Transactions on Ultrasonics, Ferroelectrics, and Frequency Control*, vol. 65, no. 6, pp. 979–990, 2018.

[13] N. A. Strnad, B. M. Hanrahan, D. M. Potrepka, and et al., "Growth of thin film ferroelectric pzt, pht, and antiferroelectric pho from atomic layer deposition precursors," *Journal of the American Ceramic Society*, vol. 104, no. 3, pp. 1216–1228, 2021.